Journal of Manufacturing Processes 136 (2025) 305–315

Contents lists available at ScienceDirect

Journal of Manufacturing Processes

journal homepage: www.elsevier.com/locate/manpro

Investigation of microstructure and mechanical properties of welds in wide stiffened panels from an innovative multi-container extrusion technology

Zhe Zhang [a], Jiaxin Lv [b,*], Chenpeng Tong [b], Zhusheng Shi [a], Jianguo Lin [c]

[a] Department of Mechanical Engineering, Imperial College London, London SW7 2AZ, UK
[b] Department of Mechanical Engineering, The Hong Kong Polytechnic University, Hung Hom, Kowloon, Hong Kong
[c] Department of Industrial and Systems Engineering, The Hong Kong Polytechnic University, Hung Hom, Kowloon, Hong Kong

ARTICLE INFO

Keywords:
Multi-container extrusion
Aluminium stiffened panels
Welding quality

ABSTRACT

The emerging multi-container extrusion, known for its notable advantage of low extrusion force requirements, offers an opportunity to produce profiles with wider cross-sections. However, the presence of intrinsic welding defects and their impact on the profile quality have not been properly studied, which limits its wider industrial application. This study aims to characterise the weld microstructures and mechanical properties of profiles produced through multi-container extrusion by conducting a series of consecutive extrusion tests under varying temperatures and speeds, followed by post-extrusion microstructural analysis and tensile tests. The findings reveal that longitudinal weld (L-weld), formed by bonding adjacent billets, becomes indistinguishable and exhibits a uniform microstructure similar to the matrix material. In addition, a pair of transverse welds (T-welds) are formed by bonding the current billet to the previous one during the consecutive extrusion process, with their gap narrowing along the extrusion direction. Microscopically, T-welds are distinct, with their width increasing with the number of consecutive extrusions, due to their differing microstructure compared to the matrix material. Macroscopically, T-welds demonstrate much lower welding quality compared with L-weld, as evidenced by all tensile specimens with welds fracturing at the T-weld without displaying the necking seen in specimens without welds. Furthermore, in specimens without welds, representing the matrix material area of the extruded profile, yield strength (YS) and ultimate tensile strength (UTS) are more sensitive to extrusion speed, while elongation is more affected by extrusion temperature.

1. Introduction

Wide aluminium alloy stiffened plates, known for their excellent overall performance as lightweight structural components, have extensive applications in various fields, such as aerospace, navigation and architecture [1,2]. Aluminium stiffened panels are generally manufactured by extrusion [3]. However, the required extrusion force is significantly high for extruding wide and thin profiles, which limits their widespread applications. Recently, a multi-container extrusion technology was proposed [4,5], which reduced the extrusion ratio through replacing a single large billet with multiple smaller billets, thereby effectively reducing the extrusion force. This technology has been successfully utilised in manufacturing wide profiles in a lab-scale environment [4,6]. In these studies, the extrusion force for the wide profiles was significantly reduced by 70 % - 85 % compared to conventional extrusion methods.

In the multi-container extrusion process, multiple billets are extruded into channels of the upper die, welded together in the welding chamber, and formed into large integral panels. Therefore, longitudinal welds (L-welds) inevitably form during this process potentially leading to poor mechanical properties in the final extrudate. L-weld defects also occur in conventional porthole extrusion process due to its intrinsic deformation mechanism where the material from a single billet is initially split into several parts and then welded together. The intrinsic presence of L-welds can degrade mechanical properties. Donati et al. [7,8] found in uniaxial tensile tests of AA6082 profiles produced by conventional extrusion that while the ultimate tensile strength (UTS) of profiles with defect-free L-welds is comparable to that of profiles without welds, the ductility, measured by area reduction of fractured specimens, is lower than in the base material. This ductility can be enhanced by optimising extrusion parameters like speed and pressure. Bakker et al. [9] observed similar outcomes, noting that ductility

* Corresponding author.
E-mail address: j.lv19@imperial.ac.uk (J. Lv).

https://doi.org/10.1016/j.jmapro.2025.01.073
Received 28 August 2024; Received in revised form 22 January 2025; Accepted 24 January 2025
Available online 30 January 2025

decreases due to L-welds in dispersoid-rich, non-recrystallised alloy 620 but remains stable in dispersoid-free, recrystallised alloy 621, a difference attributed to the microstructural texture and preferential damage path in the base material [10]. To eliminate the negative effect of L-welds, extensive research has been conducted on the L-welds in the porthole extrusion, focusing on the bonding mechanism [11], evaluation of welding quality [12], microstructural morphology of the welding zone [13], and optimisation of the welding chamber [14] to ensure a qualified extrudate quality. This long-term and comprehensive research has supported the development of porthole extrusion into a mature manufacturing technology. Similarly, the development of multi-container extrusion requires an in-depth analysis of L-welds. Given the different deformation mechanisms between multi-container extrusion and porthole extrusion, their L-welds could possess different properties. This difference renders the research outcomes of L-welds in porthole extrusion not entirely applicable to multi-container extrusion. Therefore, a focus on the L-welds specifically in multi-container extrusion is imperative. Recently, Lv et al. [15] studied the performance of L-welds in multi-container extrusion and found that the L-welds became indistinct 83 mm from the extrudate front end and completely disappeared at further distances. However, the characteristic of L-welds and the related microstructural evolution in multi-container extrusion are yet to be deeply analysed.

Transverse welds (T-welds) form in consecutive extrusion processes where new billets are added to the container in succession for mass production [16]. Therefore, in addition to L-welds, advancing multi-container extrusion to mass production also requires a deep understanding of T-welds. Many studies have evaluated the effects of L-welds and T-welds on the mechanical properties of extrudates. Unlike L-welds, T-welds often lead to a more significant reduction in mechanical properties, as they are frequently contaminated by oxides and dust [17]. This reduction is observed along the entire length of the T-weld and varies according to the T-weld transition stage [18,19]. Consequently, the extrudate part containing T-welds are normally cut off in industrial practice, causing a high percentage of material waste up to 20 % [20]. Recent advancements in research have focused on predicting and improving the T-weld quality through experimental analysis and modelling establishment to make the T-welded extrudate part useful in future [21,22]. For the present multi-container extrusion, how this new material deformation mechanism affects the performance of T-welds is still unknown and hard to predict. For example, low extrusion ratio, a feature of multi-container extrusion, has been found to favour the reduction the T-weld length and hence improve its overall quality except for the front end [23]. However, this low extrusion ratio may also cause low bonding pressure of T-welds, leading to bad welding quality. These speculations all need to be verified experimentally. In summary, a systematic study is required for both L-welds and T-welds in multi-container extrusion process to enable the future application of this technology in industry.

The main factors that affect welding quality during extrusion are temperature and speed. It is believed that elevated temperature can promote atomic diffusion, and aid in void closure [24,25]. A higher extrusion temperature contributes to the improvement of welding quality with an enhancement of mechanical properties [26,27]. However, there is a debate on how extrusion speeds affect the welds. Some researchers suggest that a higher extrusion speed may reduce welding duration at the welding interface, and potentially lead to longitudinal weld tearing, thereby weakening welding quality and mechanical properties [28,29]. Conversely, other researchers believe that a higher extrusion speed can enhance welding quality by increasing the temperature within the welding region, and thus, facilitating void closure at the welding interface [5,30]. However, the new extrusion technology, multi-container extrusion, currently lacks systematic research on the effect of extrusion temperature and speed on both L- and T-welds. Such research is of significance for ensuring the performance control of welds in practical production, thereby expanding the applications of multi-container extrusion.

Therefore, this study aims to clarify the characteristics of longitudinal and transverse welds during consecutive multi-container extrusion processes and to examine the effects of extrusion parameters, including temperature, speed, and consecutive extrusion number, on weld microstructure and mechanical properties. AA6061 stiffened profiles were extruded under various temperatures and speeds in a series of consecutive multi-container extrusion experiments. Microstructure evolution in the welds was characterised using optical microscopy (OM) and electron backscatter diffraction (EBSD), while the mechanical properties were evaluated through tensile testing.

2. Experimental setup for three-container extrusion system

2.1. Materials and stiffened panel geometry

The material used in extrusion experiments is homogenised AA6061 aluminium alloy, with its chemical compositions shown in Table 1. Cylindrical billets with 36 mm in diameter and 110 mm in length were cut from the as-homogenised ingot. The microstructural morphology of the billet material on the plane perpendicular to the billet length direction, which aligns with the cross-section used for microstructural observations of the extruded profiles in Sections 3 and 4 (ND-TD plane) is shown in Fig. 1. It reveals that equiaxed grains are uniformly distributed on the observation plane with an average grain size of 92.48 μm. A few low-angle grain boundaries (subgrain structures), represented by grey lines, are visible within the grains, resulting in an average subgrain size of 84.21 μm.

Fig. 2 shows the designed cross-sectional dimensions and a photo of the actual extruded AA6061 stiffened plate, with 177 mm in width and 3 mm in thickness for the base plate. Six ribs are evenly distributed across the plate, spaced 27 mm apart, and with 12 mm in height and 2.5 mm in thickness.

2.2. Three-container extrusion system and test procedure

Fig. 3 shows the multi-container extrusion dies for manufacturing stiffened panels, which have been optimised based on previous research [5]. As shown in Fig. 3(a), the die set includes a container, an upper die and a lower die. A tiny step of 5 mm in the container is utilised for stripping off the oxide surface of billets. The channels in the upper die are utilised to expand the materials, and the welding chamber in the lower die features for welding these three material flows. Initially during extrusion, the billets are upset and the surfaces are peeled by the tiny step, and then the billets deform plastically upon entering the channels, gradually shrinking in height and spreading in width. Following this, the material enters, contacts each other, and fills the cavity of welding chamber. Ultimately, the material is forced through the die bearing and out of the orifice, forming the desired profile. In the extrusion die set, some holes were added for cartridge heating elements and thermocouples to heat and control the temperature, and some holes were machined for locating pins and bolts to assemble the extrusion system, as shown in Fig. 3(b). The extrusion dies were made of AISI H13 tool steel and tempered to a hardness of 50 HRC.

Fig. 4 shows the extrusion systems for the multi-container extrusion. In addition to the extrusion die set, the system requires other facilities, including a 2500 kN Instron press for providing the extrusion force required, the extrusion frame for holding the extrusion dies, and the heating system for providing target extrusion temperature. Temperatures of the extrusion dies, billets, and container were monitored using

Table 1
Chemical compositions of the as-homogenised AA6061 aluminium alloy billets.

Element	Si	Mg	Fe	Cu	Mn	Cr	Zn	Ti	Al
(wt%)	0.6	0.9	0.5	0.3	0.1	0.1	0.1	0.1	Bal.

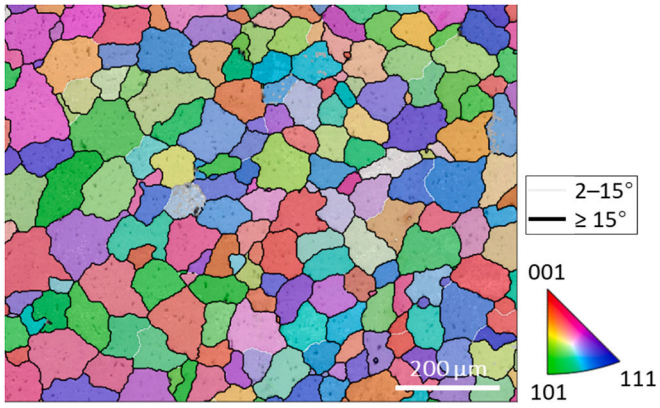

Fig. 1. Microstructure of billet material on the plane perpendicular to billet length direction.

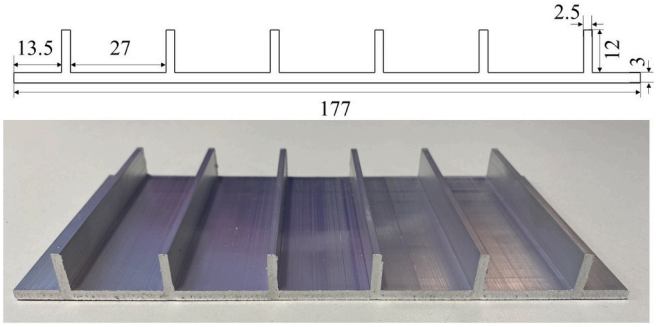

Fig. 2. Dimensions of profile designed and the actual extruded AA6061 stiffened panel (unit: mm).

temperature controllers. To deliver the required extrusion force and the retraction force afterwards, three punches were connected to the top plate of the extrusion frame, which were further linked to the Instron press.

To systematically investigate extrusion behaviour and extrudate welding quality, ten extrusion tests, under different conditions, were conducted consecutively, without cleaning out the residual material to simulate the mass production condition in industry. The extrusion was conducted under five combinations of billet temperature and extrusion speed, and the details of condition are listed in Table 2. The procedure was as follows: 1) The extrusion tools were heated to the target temperature and then held for 1 h to ensure uniform and stable temperature. In the meantime, three aluminium billets were heated and soaked in a furnace to the target temperatures. 2) Then the three heated billets were fast placed in their respective containers and were extruded with three punches at the required extrusion speed. 3) Once one extrusion test was completed, the punches were halted and repositioned and a 472 mm long profile was extruded. 4) Subsequent tests were performed by repeating these steps. Each extrusion condition was tested twice, with the profile cut off and air-cooled to room temperature after every two tests. Since profiles were cut off after every two tests, the full extrusion length of the 1st, 3rd, 5th, 7th, and 9th profiles can be collected for analysis. In contrast, portions of the second extrusions (2nd, 4th, 6th, 8th, and 10th profiles) remained in the extrusion equipment, resulting in limited region available for post-extrusion examination. Additionally, transverse welds (T-welds), the main focus in this study, were not formed in the 1st test but were present in all subsequent tests. Therefore, considering the availability of T-welds and sufficient extrusion length for analysis, samples produced from 2nd, 3rd, 5th, 7th, and 9th tests were chosen for the investigation of microstructure and mechanical properties.

2.3. *Post-extrusion examinations: Microstructure characterisation and tensile test*

Since subsequent billets are inserted directly after an extrusion test, it is inevitable that both longitudinal welds (L-welds) and transverse welds (T-welds) are formed at the same time, as shown in Fig. 5(a). L-welds form between adjacent billets, while T-welds form between consecutive extrusion billets, creating a 472 mm distance between the tips of each T-weld, as illustrated in Fig. 5(a). The T-welds were not visible to the naked eye, and the tip of the T-weld, marked as the 0 mm line (red dashed line), can be identified relative to the commonly known ‘stop mark’. The stop mark (green dashed line) forms due to localised material deformation at the extrusion die orifice when the extrusion machine pauses to load additional billets during the consecutive extrusion process. For each extrusion round, the extrudate begins at the stop mark with the exit of the remaining billet material in the die cavity from the previous run, followed by the current billet material, forming a T-weld between them. Therefore, as shown in Fig. 5(a), the distance between the stop mark and 0 mm line can be calculated based on the volume of the extrusion die cavity. Using this calculation, the position of the invisible 0 mm line was estimated as approximately 167 mm away from the stop mark and was subsequently confirmed through

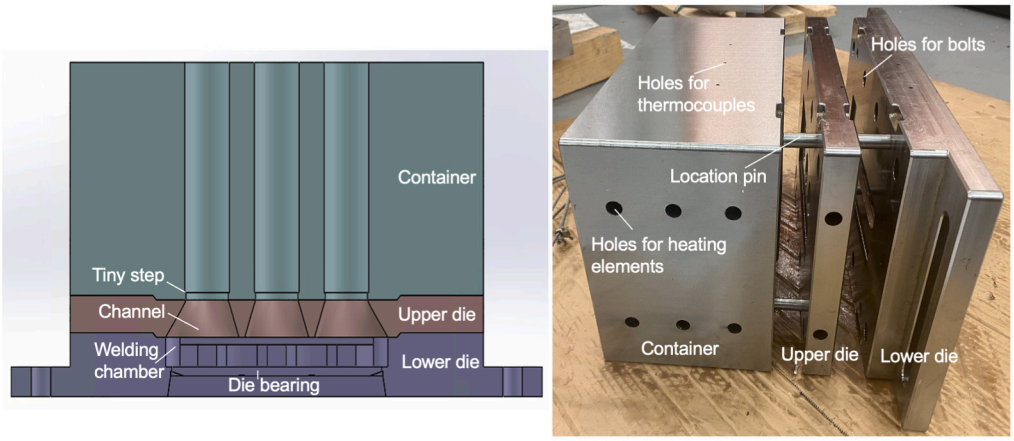

(a) Cross-sectional view of the modified extrusion die (b) Manufactured extrusion dies

Fig. 3. The multi-container extrusion dies.

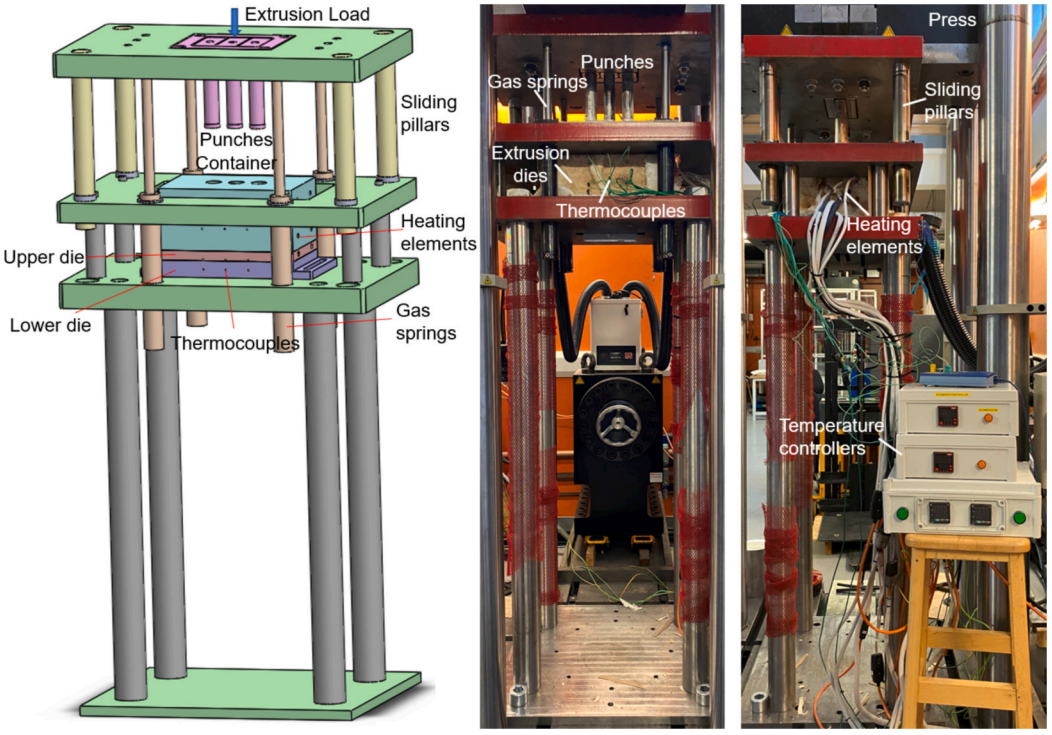

Fig. 4. Extrusion system consisting of dies, punches, heating system, extrusion press and other supporting components.

Table 2
Extrusion process parameters for experiments.

Extrusion test No.	1st&2nd	3rd&4th	5th&6th	7th&8th	9th&10th
Extrusion temperature (°C)	480	480	480	450	510
Extrusion speed (mm/s)	0.5	1	2	1	1

microstructural observation. In this study, the extrusion direction, transverse direction and normal direction are respectively labelled as ED, TD and ND.

After extrusion, six ribs were removed from the stiffened panels to facilitate two phases of the post-extrusion examinations. Notably, these examinations were conducted 1.5 months after extrusion, during which natural ageing occurred. The first phase aimed to investigate the weld evolution pattern through five OM tests on the profile cross-sections (ND-TD) at different positions along ED, in the profile produced by the 9th extrusion test, as shown in Fig. 5(a). These specimens were spaced at 100 mm intervals from the 0 mm line, which is tangent to the head of the T-welds curve, and were positioned at 0, 100, 200, 300, and 400 mm, respectively. The second phase focused on analysing the microstructure within the welding zone and its impact on the overall mechanical properties of the extrudate. This phase includes OM, EBSD and tensile tests on five profiles extruded under different temperature and speeds. As illustrated in Fig. 5(b), OM and EBSD specimens were taken 100 mm from the 0 mm line, and seven tensile specimens were prepared nearby, four of which with welds and three without.

For microstructure tests (OM and EBSD), the rectangular specimens (20 mm × 4 mm × 3 mm) were taken from the position between two tensile specimens with welds. OM observation was performed on the specimen taken along the cross-section (ND-TD) with an area of 4 mm × 3 mm, and these samples were ground up to 4000 grits, polished up to 1 μm and then etched with Keller's reagent for 60 s. According to OM observation results, the location of welds in the samples were determined and marked. Following this, the surfaces of the samples were re-prepared for EBSD analysis. Specifically. the sample surfaces were re-ground and re-polished to 1 μm, and electropolished using an electrolyte composed of 92 % ethanol and 8 % perchloric acid at a voltage of 20 V for 30 s. The EBSD uses an Oxford Symmetry detector in a TESCAN Scanning Electron Microscope (SEM). The EBSD data were collected under a beam voltage of 25 kV, beam current of 10 nA, working distance of 10 mm, and a step size of 1 μm. The grain structures of the specimens were analysed using AZtecCrystal software.

For tensile tests, two groups of tensile specimens were used: one group with four specimens where the welds were located in the middle of the gauge length, and another group with three specimens from the base plates without welds. This setup was designed to compare the mechanical properties of extrudates with and without welds. The dimensions of tensile specimens are also shown in Fig. 5(b). The tensile samples were tested at room temperature with a strain rate of 0.0005 s^{-1}.

3. Investigation of weld evolution and characteristics

3.1. Weld evolution during the same extrusion test

Fig. 6 shows the weld evolution on the cross-sections of the profiles extruded during the 9th test at a temperature of 510 °C and speed of 1 mm/s. The sampling locations are spaced at 100 mm intervals along the extrudate, from 0 to 400 mm away from the 0 mm line that represents the tangent to the head of the T-weld curve as shown in Fig. 5. At 0 mm (Fig. 6(a)), the L-weld and T-welds generated from previous extrusion tests are converge in the centre, forming a middle welding zone. At 100 mm (Fig. 6(b)), a pair of T-welds emerge on the sides of the observation area, indicating the material from current billet (the 9th billet) is starting to flow into the material from 8th billet. As the distance increases to 200 mm and 300 mm (Fig. 6(c) and Fig. 6(d)), the gap between the T-welds narrows, showing an increased presence of the current billet's material in the cross-section. By 400 mm (Fig. 6(e)), the T-welds fully merge into the middle welding zone. This entire weld evolution indicates that at the start of each consecutive extrusion test,

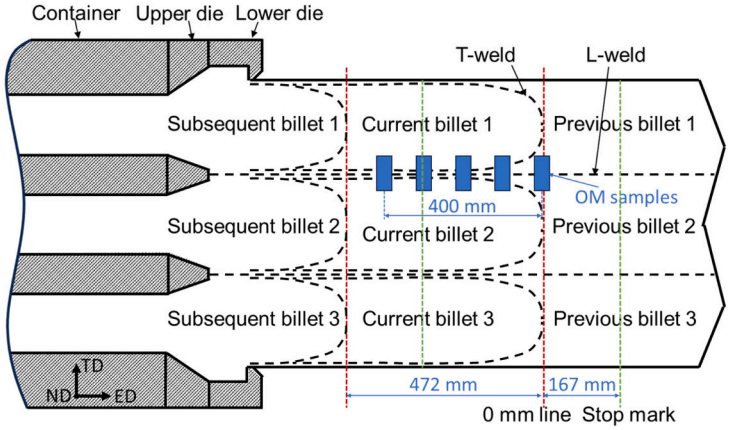

(a) Formation process of longitudinal welds (L-welds) and transverse welds (T-welds)

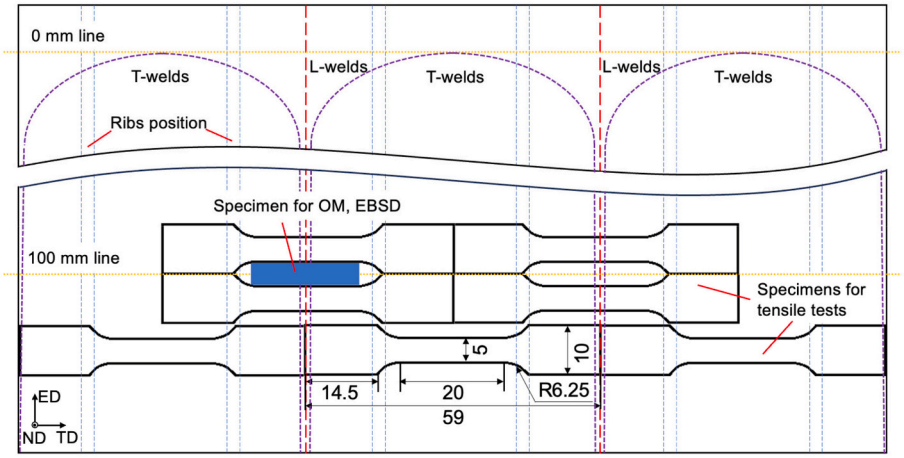

(b) The positions of specimens for OM, EBSD and tensile tests (unit: mm).

Fig. 5. Schematic of the formation process of welds and the positions of specimens for characterisation.

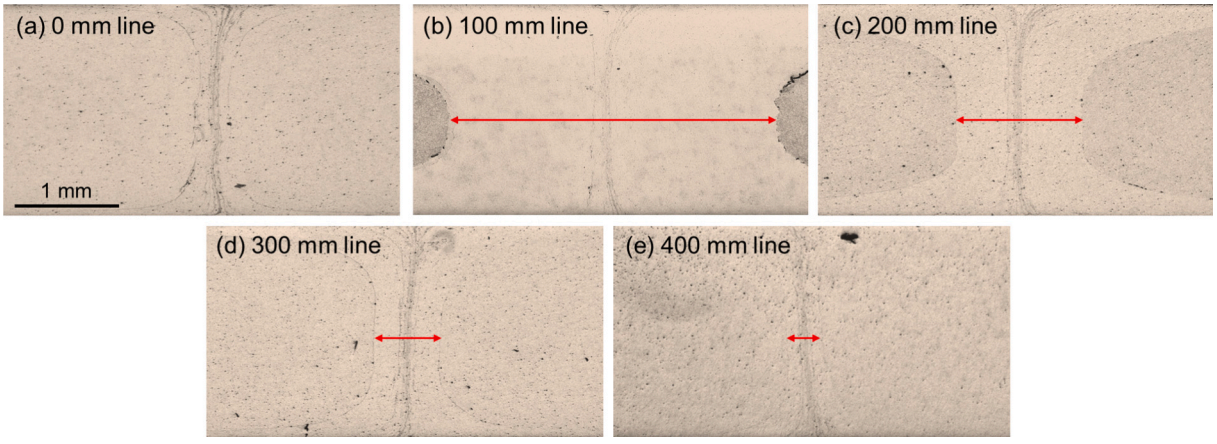

Fig. 6. Weld appearance at different positions (located 0, 100, 200, 300, and 400 mm from 0 mm line shown in Fig. 5) of the profile extruded in the 9th extrusion test. The red line indicates the distance between the pair of newly formed T-welds. (For interpretation of the references to colour in this figure legend, the reader is referred to the web version of this article.)

the current billet material gradually displaces the previous billet material until it completely occupies the cross-section of the extrudate.

3.2. Weld characteristics at various extrusion conditions

Fig. 7 shows the characteristics of welds on the cross-sections (ND-TD) of the profiles from different extrusion tests (2nd, 3rd, 5th, 7th and 9th tests), covering various temperatures and speeds. In the 2nd extrusion test with an extrusion temperature of 480 °C and an extrusion speed of 0.5 mm/s (Fig. 7(a)), the cross-sections of the extrudate feature two different weld types: longitudinal weld (L-weld) and transverse weld (T-weld). There are two convex T-welds symmetrical on either side of a

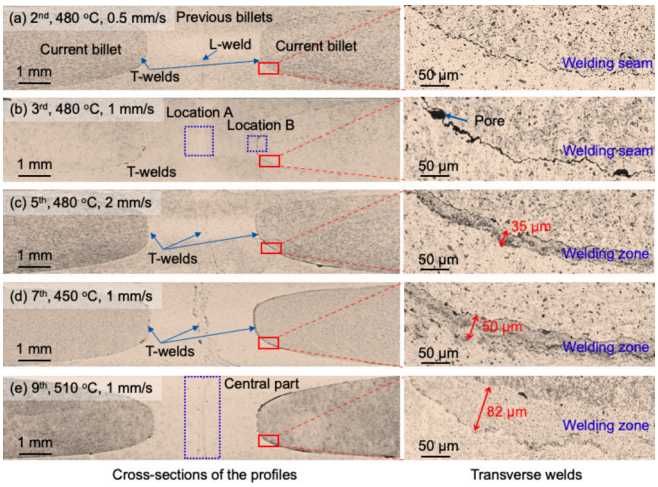

Fig. 7. Welds appearance in the cross-sections (ND-TD) of the extruded profiles from different extrusion tests, showing the evolution of transverse welds. Locations A and B are selected areas for each specimen for EBSD analysis.

straight L-weld, with the bulge of the T-weld convex curve facing the L-weld. The L-weld shows a lighter thin seam, while the T-weld exhibits a slightly darker thin seam. The cross section of the profile from the 3rd extrusion test at 480 °C and 1 mm/s is shown in Fig. 7(b). The L-weld is almost invisible, while the two pairs of T-welds become thicker, with some pores along the seam. As the extrusion test progress, the L-welds remain indistinguishable, while the T-welds evolve from a seam to a wider welding zone, with its width increasing over time. These features appear to be independent of the extrusion parameters but related to the number of extrusion cycles. Measurements of the weld zone width for panels extruded in the 5th, 7th, and 9th tests show the widths being approximately 35, 50, and 82 μm, respectively.

Fig. 8 is an enlarged view of the central area on the cross-sections of the profiles shown in Fig. 7. As the extrusion tests progress, the L-weld becomes gradually less visible, while the number of T-welds accumulates. In the 9th extrusion test, T-welds from previous billets are still visible, indicating that the duration of T-welds is very long. Additionally, the T-welds become less prominent as they approach the central area near the L-weld. This suggests that while T-welds are initially

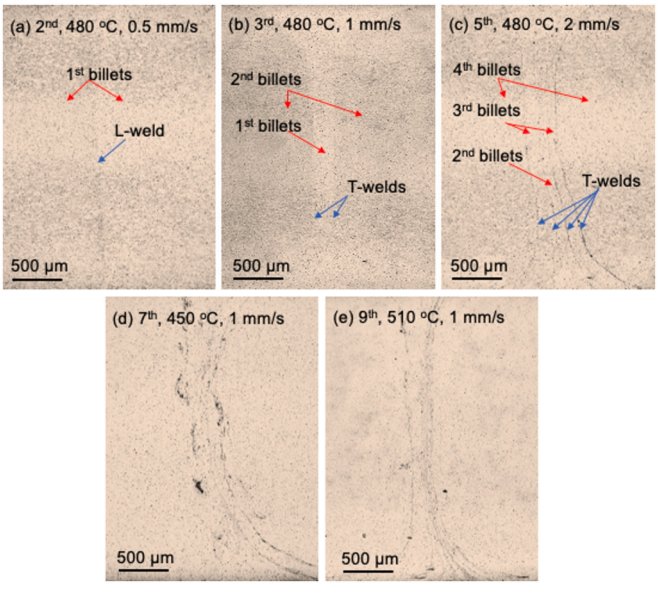

Fig. 8. Welds appearance including L-welds and T-welds in the central area of the specimens shown in Fig. 7 for different extrusion temperatures and speeds.

prominent at the starting point (location B in Fig. 7) with obvious welding seam/zone for the current cycle of extrusion, they move towards the central area and gradually become less distinct during the extrusion process. This phenomenon indicates the persistence and slow transition of T-welds through consecutive extrusion tests, not sensitive to the specific changes in extrusion parameters.

According to Fig. 7 and Fig. 8, the weld characteristics can be summarised. For L-weld, it becomes indistinguishable after the 2nd extrusion. On the other hand, the width of T-welds is significantly influenced by the number of consecutive extrusion tests with minimal relationships with extrusion temperature and extrusion speed. The possible reason is that after each extrusion test, some material remains on the inner wall of the extrusion containers and dies, due to the difference in diameter between the punch and the container. When the subsequent billet is upset at the beginning of the extrusion process, some previous material will adhere to the surface. As the number of extrusion tests increases, the amount of material attached between new and remaining material increases, thereby increasing the area of the welding zone.

4. Variation of grain structures in welding area

4.1. Microstructure in the middle welding zone

Fig. 9 shows the EBSD inverse pole figure (IPF) maps, with respect to the extrusion direction on the cross-sections (ND-TD) of the profiles at location A (central area) in Fig. 7, for profiles extruded from different extrusion tests with various extrusion temperatures and speeds. The white lines represent low-angle grain boundaries (LABs, with misorientation angles in the range of $2° \leq \theta < 15°$), while the black lines indicate high-angle grain boundaries (HABs, with misorientation angles of $\theta \geq 15°$). The grains at location A have a strong orientation, predominantly in [111]//ED direction. However, there are grains oriented in [001]//ED direction on both sides of the thickness as shown in the regions marked by the dashed yellow rectangles, likely due to the shear strain generated by friction between the material and the die bearing. Only few vertically arranged grains with the [001]//ED orientation are observed near the L-welds, but these oriented grains gradually disappear as extrusion progress. Furthermore, although the L-weld and T-weld appear as light thin seams in Fig. 8 when observed by OM, these welds are hardly visible in EBSD maps. Instead, the microstructure in location A in all situations shows quite uniform structure when comparing areas with and without welds, indicating that the welds cause minimal impact on the microstructure.

On the other hand, the extrusion parameters significantly affect the microstructure in the extrudate, as evidenced in Fig. 10, which shows the relationship between average subgrain size and extrusion temperature and speed. In Fig. 10(a), at a constant extrusion temperature of 480 °C, the average subgrain size decreases with increasing extrusion speed. Specifically, the average subgrain size are 23.86, 15.85, and 15.76 μm, respectively for 0.5, 1, and 2 mm/s. These results indicate that higher extrusion speeds tend to refine the subgrain structure, resulting in smaller subgrain size. This refinement is attributed to the increased dislocation densities at higher speeds, as less time is available for dynamic recovery, promoting the formation of finer subgrains. Additionally, the reduced time for recrystallisation contributes to a decrease in subgrain boundary area, further reducing subgrain size [31]. In addition, the similar subgrain sizes observed at 1 mm/s and 2 mm/s suggest that higher extrusion speeds may increase the material temperature, which could lead to subgrain growth. In Fig. 10(b), at an extrusion speed of 1 mm/s, the average subgrain size increases with increasing temperature, rising from 11.63 μm at 450 °C to 46.17 μm at 510 °C. This potential reasons for this trend are as follows: Firstly, higher temperatures enhance grain boundary mobility, which promotes atom diffusion, leading to grain boundary migration and subgrain growth [32]. Additionally, higher temperatures accelerate dynamic recovery, recrystallisation, and grain growth rates, all of which contribute to the observed

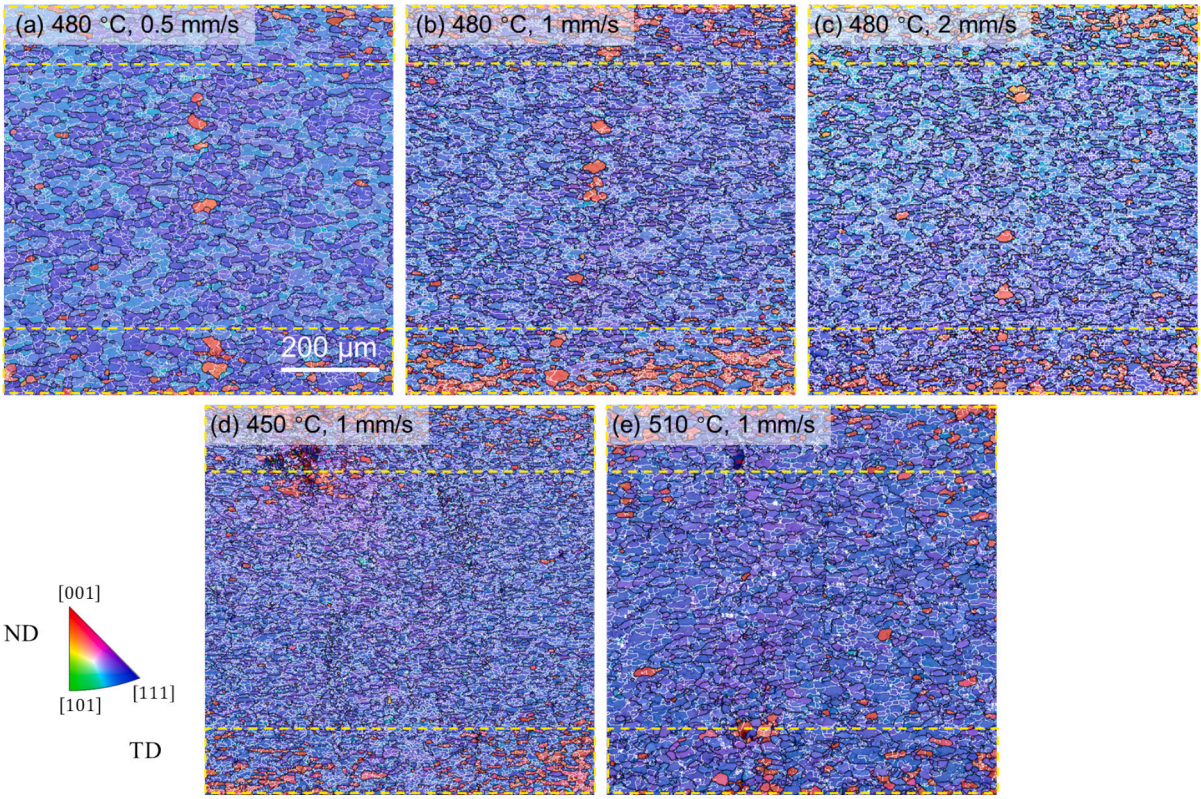

Fig. 9. EBSD IPF maps in location A (central area) shown in Fig. 7, showing grain structures at different extrusion temperatures and speeds.

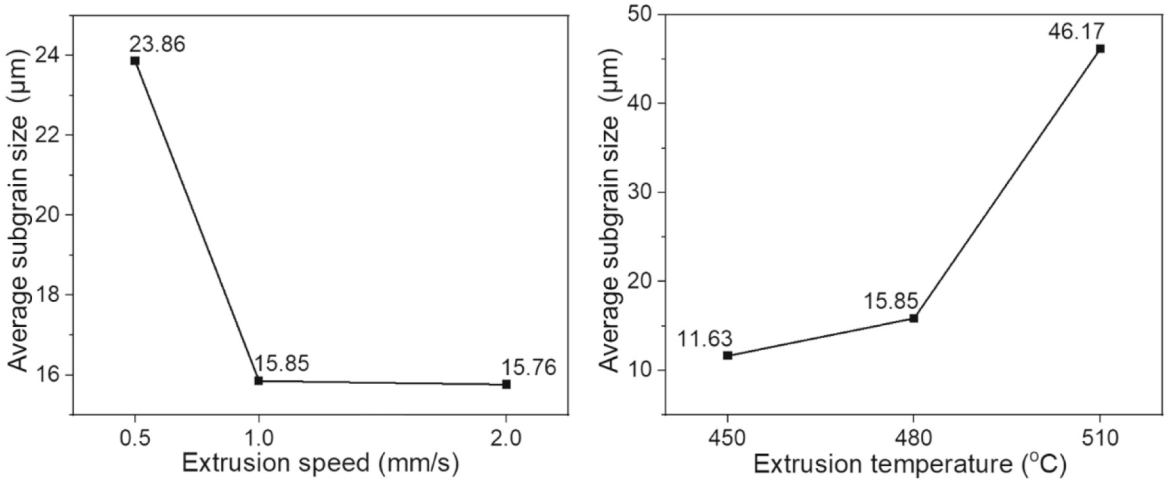

(a) At same extrusion temperature of 480 °C (b) At same extrusion speed of 1 mm/s

Fig. 10. The relationship of the average subgrain size with different extrusion speeds and temperatures in location A.

increase in average subgrain size [33].

4.2. Microstructure of T-weld

Fig. 11 shows the EBSD inverse pole figure maps at location B (marked in Fig. 7), where the T-weld originates, for specimens from different extrusion tests. The left side of the T-welds is the n^{th} billet, and the right side is the $(n + 1)^{th}$ billet. The EBSD maps here are quite different from the results at location A (Fig. 9), where the T-weld is very obvious and distinct from the matrix microstructure. Specifically, in the 2nd and 3rd tests, the T-weld appears as a seam. As the extrusion progresses to the 5th, 7th, and 9th tests, the T-weld transforms into a zone and the width of this zone increases, consistent with the OM results shown in Fig. 7. Furthermore, the grains in the welding zone are significantly smaller than those in the matrix material, suggesting that significant recrystallisation occurs at the T-weld. The degree of recrystallisation and the affected area grow with continued extrusion. This phenomenon might be attributed to the fact that although each extrusion cycle involves welding the end of the previous billet to the beginning of a new one, these processes are not entirely independent. The cumulative effects can influence subsequent welding processes, leading to finer grain refinement and more apparent weld zones as the number

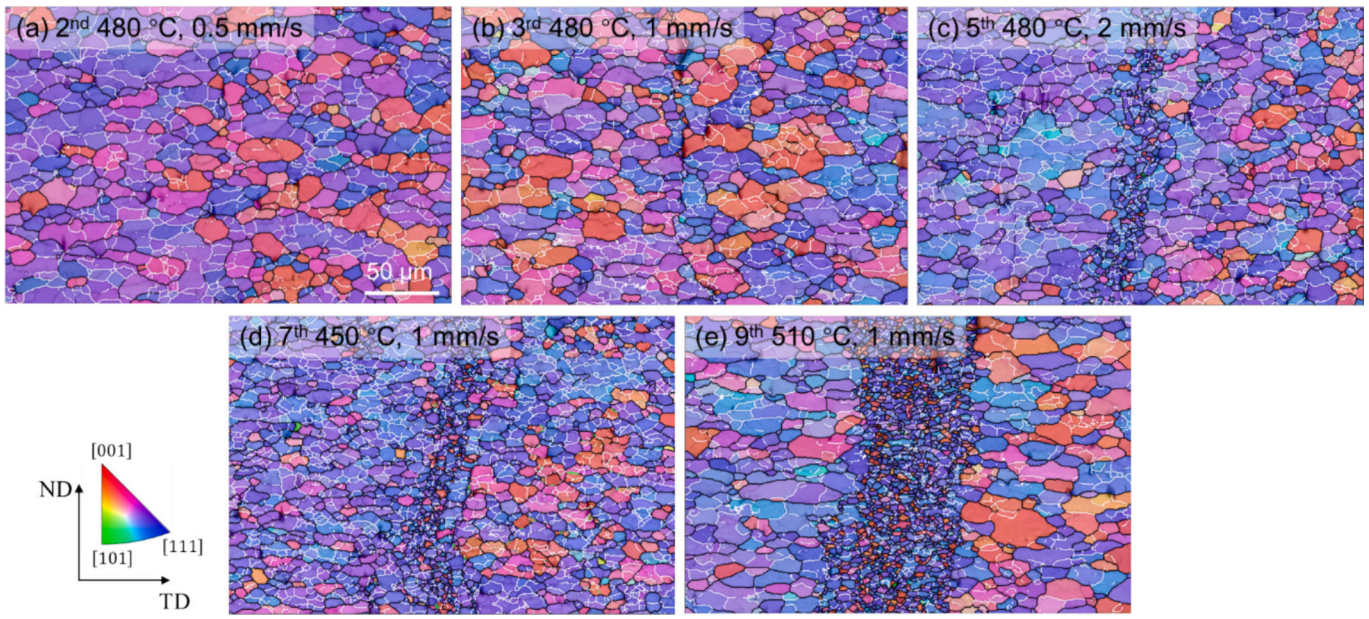

Fig. 11. EBSD IPF maps in location B shown in Fig. 7, showing T-welds and grain structures at different extrusion temperatures, speeds and extrusion cycles.

of extrusions increases. However, these obvious welding zones will eventually become invisible as they gradually move towards the central part near the L-weld, where higher pressure can cause a better and more uniform microstructure.

Fig. 12 shows the misorientation angle distribution in location B along with the fractions of HABs and LABs. With increasing misorientation angle from 2°, the relative frequency initially decreases in the LABs region, then stabilises (20°-40°), and finally experiences an increase to a peak and decreases again in the HABs region. The proportion of LABs increases with the rising extrusion speed at a consistent extrusion temperature, whereas it decreases with the increasing extrusion temperature at a constant extrusion speed. When the extrusion speed is increased, the increased strain rate promotes the movement of dislocations, leading to formation of new subgrains with LABs. Conversely, when extrusion temperature is increased at constant extrusion speed, it influences the material's recrystallisation kinetics. A higher temperature accelerates the recrystallisation process, leading to the formation of recrystallised grains. As a result, the proportion of HABs increases and the proportion of LABs decreases.

5. Assessment of mechanical properties and discussion

Fig. 13 shows the engineering stress-strain curves of the billet material and profiles extruded at different conditions, with solid lines

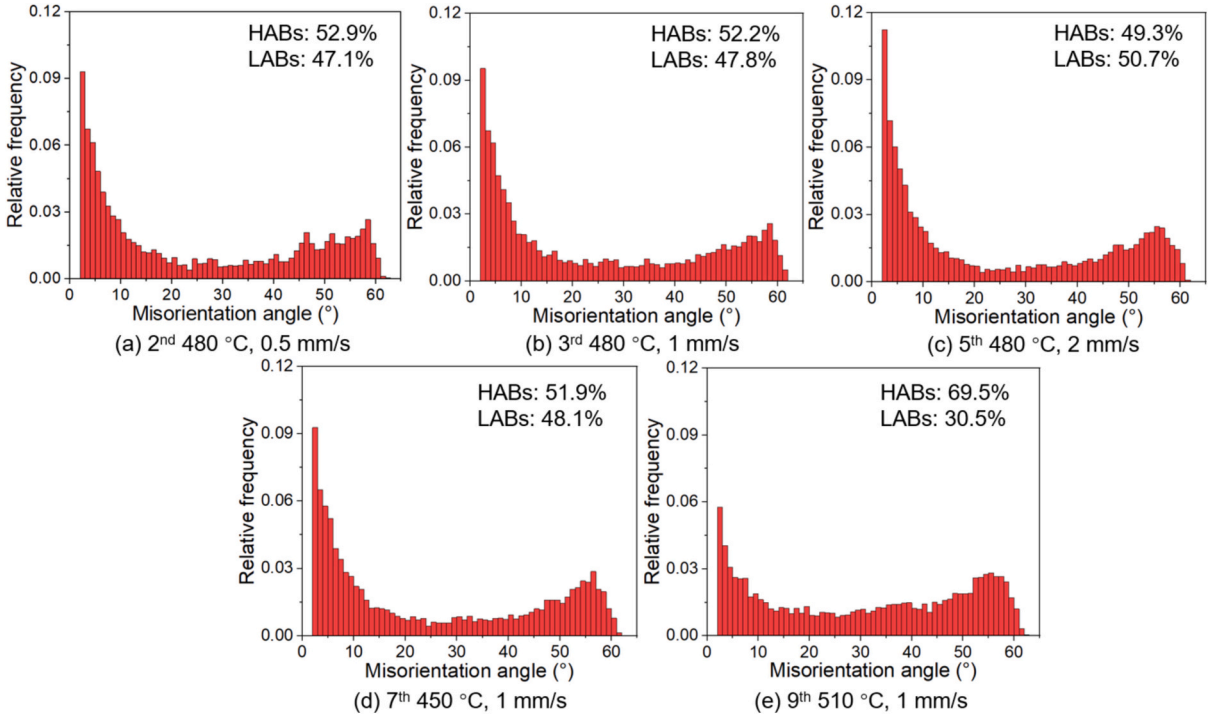

Fig. 12. Misorientation angle distribution in location B at different extrusion temperatures and speeds.

representing tensile specimen without welds and dashed lines representing those with welds. The corresponding mechanical properties are detailed in Fig. 14. The initial homogenised billet has the yield strength (YS) of 56.2 MPa, ultimate tensile strength (UTS) of 129.4 MPa and elongation of 34 %, respectively, consistent with standard AA6061-O material [34]. Compared with the base material, the extruded profiles without welds show higher YS and UTS and lower elongation.

For specimens without welds, a higher extrusion speed leads to higher strengths, as shown in Fig. 13(a). For instance, the UTS and YS increases from around 140 MPa and 68 MPa at 0.5 mm/s to 160 MPa and 80 MPa at 2.0 mm/s, while the total elongation (TE) remains relatively unaffected by extrusion speeds. This may be due to the increased substructures at higher extrusion speed, as indicated by the decreased subgrain size in Fig. 10(a), which can enhance material strengths [31]. Similarly, the increased substructures at lower extrusion temperature shown in Fig. 10(b) can enhance material strengths. However, this mechanism does not fully explain the trend shown in Fig. 13(b), where the temperature shows minimal impact on both YS and UTS, while decreasing temperature improves TE from 27 % at 510 °C to 31 % at 450 °C. Other mechanisms, such as precipitation hardening during the natural ageing after extrusion, may account for this trend [36].

Since this study mainly focuses on T-welds, which are typically scrapped in industry due to their inferior properties, Fig. 13(a) and Fig. 13(b) both show poorer mechanical properties in the welded specimens. However, previous research has demonstrated that the multi-container extruded profiles with L-welds exhibit comparable properties with those without welds [15]. In addition, despite the specimens in this study undergoing natural ageing after hot extrusion, the extruded profiles without welds do not exhibit comparable properties to standard AA6061-T4 material. This discrepancy could be due to the cooling condition during the extrusion process. The profiles cooled slowly in air to room temperature due to lab facility constraints, unable to achieve fully supersaturated solid solution (SSSS) state. As a result, the profiles extruded under various conditions exhibit lower strengths (68–80 MPa YS, 140–160 MPa UTS) and higher total elongation (27–31 %), compared to the properties of standard T4 material (145 MPa YS, 241 MPa UTS and 22–25 % TE [36]). To further assess the industrial applicability of multi-container extrusion technology, heat treatment was applied to the profile extruded at 510 °C and 1 mm/s, including solution heat treatment (SHT) at 530 °C for 2 h, water quenching, and

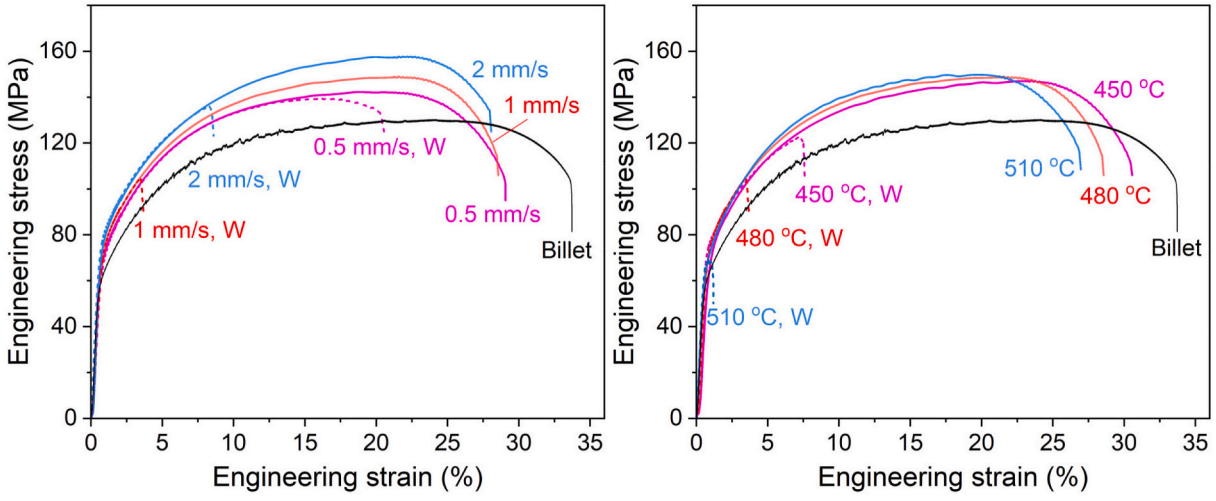

(a) Different speeds (at 480 °C) (b) Different temperatures (at 1 mm/s)

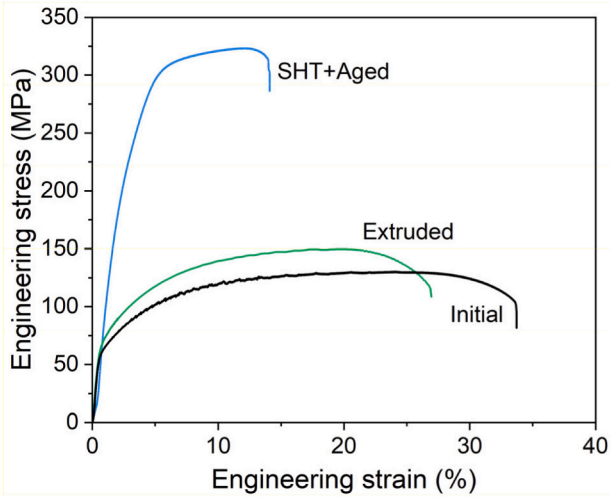

(c) Comparison between initial billet, as-extruded at 510 ℃ and 1 mm/s, and SHT + aged mateiral

Fig. 13. Tensile stress-strain curves of profiles extruded at different extrusion conditions and initial homogenised billet. The solid lines represent the tensile specimen without welds, and the dash lines represent the tensile specimen containing welds, denoted by 'W'.

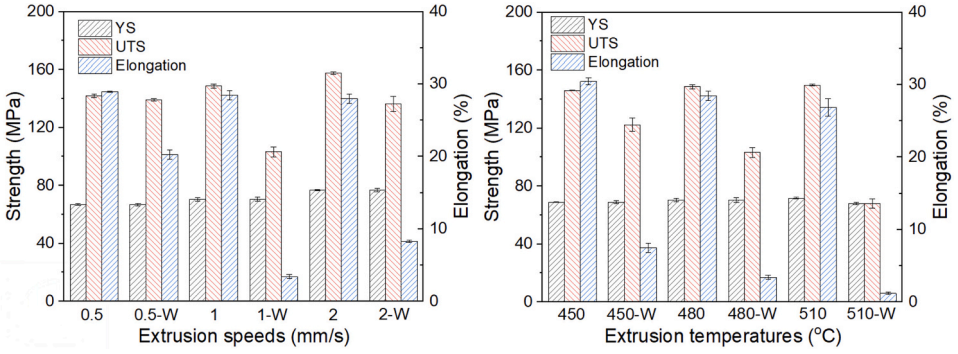

(a) Different extrusion speeds (at 480 °C) (b) Different extrusion temperatures (at 1 mm/s)

Fig. 14. Yield strength (YS), ultimate tensile strength (UTS) and total elongation (TE) of different tensile stress-strain curves. 'W' denotes specimens with welds.

ageing at 175 °C for 8 h. As shown in Fig. 13(c), the UTS of material significantly increased from 150 MPa to 323 MPa after heat treatment, demonstrating that this technology can produce Al alloy structures with superior mechanical properties comparable to conventional methods like rolling and die casting.

The specimens with welds exhibit much lower YS, UTS and TE compared with those without welds under all conditions, indicating inferior mechanical performance. As shown in Fig. 15, fractures in specimen with welds consistently occurs at the T-weld (location B in Fig. 7) without showing any ductile behaviour that is seen in the specimens without welds. This indicates that the welding quality of the newly formed T-weld is inferior compared to that of the middle L-weld and T-weld zone. This could be attributed to the presence of impurities and oxides within the bonding interfaces of the T-welds, coupled with the separation of grains by these interfaces. During tensile tests, these contaminants and disjointed grains in the T-weld regions facilitate the micro-crack initiation and propagation, leading to strain concentration and making fractures more likely at T-welds.

Fig. 16 shows the relationship between total elongation for the specimens with welds and the number of extrusion tests. It can be observed that the total elongation generally decreases as extrusion progresses, regardless of the extrusion parameters. This trend corresponds to the observation that the T-welds gradually expand from a seam to a zone with increasing extrusion test number. This indicates that a wider T-weld zone results in poorer mechanical performance potentially due to the severe defects. Additionally, the abnormally low value at the 3rd extrusion test is contributed to the pores around the T-weld (as shown in Fig. 7(b)), possibly caused by accidental impurity contamination in the billet or the container.

6. Conclusions

This study focuses on clarifying the characteristics of both longitudinal (L-welds) and transverse welds (T-welds) formed during the consecutive tests of the innovative multi-container extrusion at various temperatures and speeds. The conclusions are as follows:

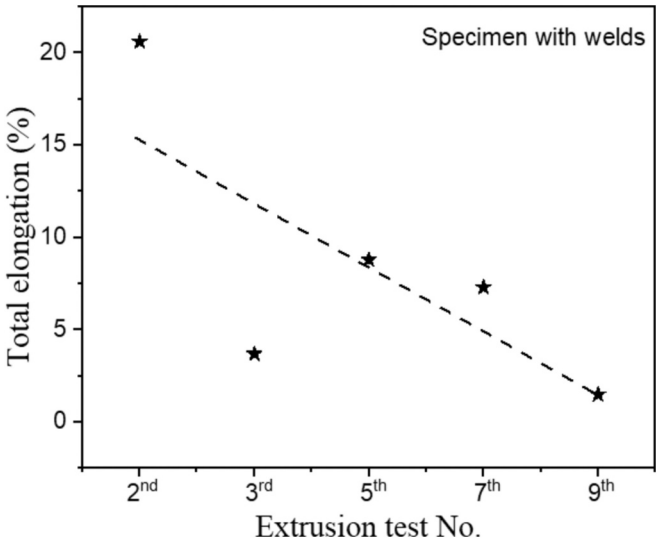

Fig. 16. Variation of total elongation (TE) with extrusion tests number for the specimens with welds.

1. L-weld becomes indistinguishable after the 2nd extrusion test, while the quantity and morphology of T-welds are markedly affected by the number of the consecutive extrusion tests. As the number of extrusion tests increases, the count of T-welds rises, making their individual differentiation increasingly challenging. Interestingly, the newly formed T-weld zone gradually widens with each additional test, expanding from a weld seam during the first three extrusion tests to a width of 82 μm. This widening is attributed to the continuous accumulation of material adhere to the inner wall of the container and die.
2. The microstructure within the welding zone can be highly influenced by extrusion conditions. At an extrusion temperature of 480 °C, the average subgrain size within the area including both L-weld and T-welds decreases from 23.86 to 15.76 μm with extrusion speeds

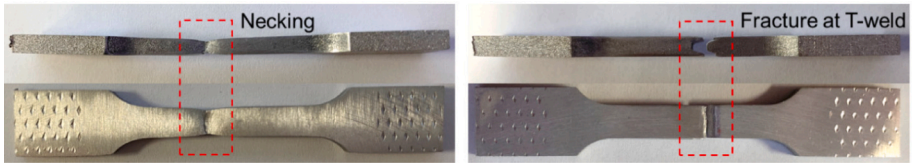

(a) Tensile specimen without welds (b) Tensile specimen with welds

Fig. 15. Tested tensile specimens with/without welds showing the fracture.

increasing from 0.5 to 2 mm/s since higher speed leads to faster generation of dislocations but allows shorter time for material softening such as dynamic recovery and recrystallisation and thereby promotes the formation of subgrain boundaries. Conversely, at a constant extrusion speed of 1 mm/s, the average subgrain size increases from 11.63 μm at 450 °C to 46.17 μm at 510 °C due to the enhanced boundary migration, recovery and recrystallisation.

3. Specimens with welds exhibit lower ultimate tensile strength (UTS), yield strength (YS) and total elongation (TE) compared to those without welds during tensile tests. For specimens with welds, all fractures occur along the newly formed T-welds rather than the middle welding zone where L-weld and previously formed T-welds accumulate. This suggests that the newly formed T-welds contain most contaminant defects before merging into the middle welding zone. This observation aligns well with the microstructural findings that the middle welding zone has a uniformly distributed grain structure, in contrast to the distinctly smaller grains found around the newly formed T-weld compared to the matrix material. For specimens without welds, increasing extrusion speed enhances UTS and YS, rising from around 140 MPa and 68 MPa at 0.5 mm/s to 160 MPa and 80 MPa at 2.0 mm/s, while having limited impact on TE. Conversely, decreasing extrusion temperature increases TE from 27 % at 510 °C to 31 % at 450 °C, while having a less pronounced effect on UTS and YS.

CRediT authorship contribution statement

Zhe Zhang: Writing – original draft, Visualization, Methodology, Investigation, Data curation. **Jiaxin Lv:** Writing – review & editing, Supervision, Methodology, Investigation. **Chenpeng Tong:** Writing – review & editing, Investigation. **Zhusheng Shi:** Writing – review & editing, Supervision, Funding acquisition, Conceptualization. **Jianguo Lin:** Writing – review & editing, Supervision, Conceptualization.

Declaration of competing interest

The authors declare that they have no known competing financial interests or personal relationships that could have appeared to influence the work reported in this paper.

Acknowledgements

The authors are grateful to the support from UK EPSRC under the Grant Agreement EP/X52556X/1 for UKRI Impact Acceleration Funding on Multi-Cylinder Extrusion Technology.

References

[1] Verma RP, Lila MK. A short review on aluminium alloys and welding in structural applications. Materials Today: Proceedings 2021;46:10687–91.
[2] P. Rambabu, N. Eswara Prasad, V. Kutumbarao, R. Wanhill, Aluminium alloys for aerospace applications, Aerospace Materials and Material Technologies: Volume 1: Aerospace Materials, 2017 29–52.
[3] Zhang Z, Zhou W, Shi Z, Lin J. Advances on manufacture methods for wide lightweight aluminium stiffened panels. In: IOP conference series: Materials science and engineering. IOP Publishing; 2022. p. 012122.
[4] Lv J, Yu J, Shi Z, Li W, Lin J. Feasibility study of a novel multi-container extrusion method for manufacturing wide aluminium profiles with low force. J Manuf Process 2023;85:584–93.
[5] Zhang Z, Zhou W, Shi Z, Lin J. Investigation of die designs on welding quality and billet material utilisation for multi-container extrusion of wide stiffened aluminium panels. Int J Adv Manuf Technol 2023:1–14.
[6] Li W, Yu J, Lv J, Shi Z, Lin J. Development of a multi-container extrusion method for extruding lightweight wide plates and sheets. In: IOP conference series: Materials science and engineering. IOP Publishing; 2022. p. 012061.
[7] Donati L, Tomesani L. Seam welds modeling and mechanical properties prediction in the extrusion of AA6082 alloy. Key Eng Mater 2008;367:125–36.
[8] Donati L, Tomesani L, Minak G. Characterization of seam weld quality in AA6082 extruded profiles. J Mater Process Technol 2007;191:127–31.
[9] den Bakker AJ, Werkhoven RJ, Sillekens WH, Katgerman L. The origin of weld seam defects related to metal flow in the hot extrusion of aluminium alloys EN AW-6060 and EN AW-6082. J Mater Process Technol 2014;214:2349–58.
[10] den Bakker AJ, Wu X, Katgerman L, van der Zwaag S. Microstructural and X-ray tomographic analysis of damage in extruded aluminium weld seams. Mater Sci Technol 2015;31:94–104.
[11] Wang Y, Zhao G, Zhang W, Sun L, Wang X, Lv Z. Interfacial bonding mechanism and length evaluation method of the longitudinal welds in the unsteady deformation process of porthole die extrusion of aluminum alloy profiles. J Mater Res Technol 2022;20:1624–44.
[12] Yu J, Zhao G, Cui W, Chen L, Chen X. Evaluating the welding quality of longitudinal welds in a hollow profile manufactured by porthole die extrusion: experiments and simulation. J Manuf Process 2019;38:502–15.
[13] Xu X, Ma X, Yu S, Zhao G, Wang Y, Chen X. Bonding mechanism and mechanical properties of 2196 Al-cu-Li alloy joined by hot compression deformation. Mater Charact 2020;167:110486.
[14] Yan P, Li F, Liu Z, Li L. Sensitivity analysis of die structural and process parameters in porthole die extrusion of magnesium alloy tube using Taguchi method. Int J Adv Manuf Technol 2022;119:8039–56.
[15] Lv J, Shi Z, Yu J, Li W, Lin J. Analysis of solid-state welding in extruding wide aluminium hollow profiles using a new three-container extrusion system. J Manuf Process 2023;94:146–58.
[16] Yu J, Zhao G, Chen L. Investigation of interface evolution, microstructure and mechanical properties of solid-state bonding seams in hot extrusion process of aluminum alloy profiles. J Mater Process Technol 2016;230:153–66.
[17] Nanninga N, White C, Mills O, Lukowski J. Effect of specimen orientation and extrusion welds on the fatigue life of an AA6063 alloy. Int J Fatigue 2010;32:238–46.
[18] A.J.d. Bakker, L. Katgerman, S.v.d.. Zwaag, analysis of the structure and resulting mechanical properties of aluminium extrusions containing a charge weld interface. J Mater Process Technol 2016;229:9–21.
[19] Bakker A. Weld seams in aluminium alloy extrusions: Microstructure and properties, in. The Netherlands: Delft University Delft; 2016. p. 108–17.
[20] Oberhausen GJ, Christopher AAA, Cooper DR. Reducing aluminum extrusion transverse weld process scrap. In: Daehn G, Cao J, Kinsey B, Tekkaya E, Vivek A, Yoshida Y, editors. Forming the future. Cham: Springer International Publishing; 2021. p. 1003–19.
[21] Oberhausen G, Cooper DR. Modeling the strength of aluminum extrusion transverse welds using the film theory of solid-state welding. J Mater Process Technol 2024;324:118254.
[22] Lou S, Wang Y, Liu C, Lu S, Liu S, Su C. Analysis and prediction of the billet butt and transverse weld in the continuous extrusion process of a hollow aluminum profile. J Mater Eng Perform 2017;26:4121–30.
[23] Hatzenbichler T, Buchmayr B. Finite element method simulation of internal defects in billet-to-billet extrusion. Proc Inst Mech Eng B J Eng Manuf 2010;224:1029–42.
[24] Wang Y, Zhao G, Sun L, Wang X, Lv Z, Sun Y. Effects of billet heating temperature and extrusion speed on the microstructures and mechanical properties of the longitudinal welds in aluminum alloy profiles with complex cross-section. Vacuum 2023;207:111578.
[25] Bai S-W, Fang G, Zhou J. Analysis of the bonding strength and microstructure of AA6082 extrusion weld seams formed during physical simulation. J Mater Process Technol 2017;250:109–20.
[26] Yu J, Zhao G, Cui W, Zhang C, Chen L. Microstructural evolution and mechanical properties of welding seams in aluminum alloy profiles extruded by a porthole die under different billet heating temperatures and extrusion speeds. J Mater Process Technol 2017;247:214–22.
[27] Jo H, Lee S, Jung C, Kim B. A non-steady state FE analysis of Al tubes hot extrusion by a porthole die. J Mater Process Technol 2006;173:223–31.
[28] Bingöl S, Keskin M. Effect of different extrusion temperature and speed on extrusion welds. Journal of achievements in materials and manufacturing engineering 2007;23:39–43.
[29] Donati L, Tomesani L. The prediction of seam welds quality in aluminum extrusion. J Mater Process Technol 2004;153:366–73.
[30] Chen L, Zhao G, Yu J. Effects of ram velocity on pyramid die extrusion of hollow aluminum profile. Int J Adv Manuf Technol 2015;79:2117–25.
[31] Jiang S, Lv J, Shi Z, Lin J. A study of dynamic recovery and recrystallisation mechanisms in aluminium alloy AA7050 at different thermomechanical processing conditions. Mater Sci Eng A 2024;914:147117.
[32] Winning M, Gottstein G, Shvindlerman L. On the mechanisms of grain boundary migration. Acta Mater 2002;50:353–63.
[33] Zhang Z, Tong C, Zhou W, Jiang S, Lv J, Shi Z, et al. Investigation of the mechanisms on the abnormal features observed in thermal-mechanical testing of AA6061 under extrusion conditions. Mater Sci Eng A 2023;884:145537.
[34] *Aluminum 6061-O*. https://asm.matweb.com/search/specificmaterial.asp?bassnum=ma6061o; [Accessed 05 11 2024].
[35] Wang Y, Zhao G, Sun L, Wang X, Lv Z, Sun Y. Effects of billet heating temperature and extrusion speed on the microstructures and mechanical properties of the longitudinal welds in aluminum alloy profiles with complex cross-section. Vacuum 2023;207.
[36] *Aluminum 6061-T4; 6061-T451*. https://asm.matweb.com/search/specificmaterial.asp?bassnum=ma6061T4; [Accessed 05 11 2024].